THE ONSET OF DEGRADATION OF A LARGE SPATTER RAMPART IN ICELAND. S. S. Sutton[1], J. A. Richardson[2,3], P. W. Whelley[2,3], C. W. Hamilton[1], S. P. Scheidt[4], K. E. Young[2], A. Höskuldsson[5], I. Jónsdóttir[5], and T. Thordarson[5], E. Gallant[6]. [1]Lunar and Planetary Laboratory, University of Arizona, Tucson, AZ USA (ssutton@lpl.arizona.edu), [2]Planetary Geology, Geophysics, and Geochemistry Laboratory, NASA Goddard Space Flight Center, Greenbelt, MD, USA, [3]Dept. of Astronomy, University of Maryland College Park, [4]Planetary Science Institute, Tucson, AZ , USA, [5]Faculty of Earth Sciences, University of Iceland, Reykjavík, Iceland, [6]School of Geosciences, University of South Florida, Tampa, Florida, USA.

Introduction: Pyroclastic deposits commonly form edifices, such as cinder cones, spatter cones, and spatter ramparts, at the vents of volcanic fissure eruptions [1]. The morphology of vent edifices is related to the eruption style and magma characteristics [2,3]. As these deposits are often associated with varied-style, monogenetic volcanism, they are generally not subject to further volcanic modification, and their subsequent degradation can be used to infer eruption characteristics. Terrestrial field studies provide the opportunity to observe the initial stages of degradation when factors contributing to morphologic change are likely to have the most in common with volcanic terrains on other rocky planets, such as edifice cooling and contraction, slope instability, and the cohesiveness of pyroclasic deposits.

Holuhraun, Iceland. The 2014–2015 Holuhraun fissure eruption in northern Iceland (64.85ºN, 16.83ºW) was the largest eruption in Iceland since 1784. The six-month eruption (August 28, 2014–February 27, 2015) deposited a lava flow 18 km long with a bulk volume of 1.44 km^3 covering 84 km^2 [4,5]. Early in the eruption, lava fountains focused at several sections along a ~2-km long fissure, forming distinct vent edifices. The largest of these, called Baugur, formed a 500-m long by 50-m high spatter rampart [6]. During buildup, Baugur featured a phase of fairly steady lava fountaining, followed by a phase of a lava lake/pond with regular but very large (>50 m in diameter) bubble bursts, which in turn was followed by a phase of relatively steady discharge from a fairly quiet lava lake/pond [5,6]. Holuhraun provides a unique opportunity to compare the onset of degradation of a large spatter rampart to its constructional dynamics.

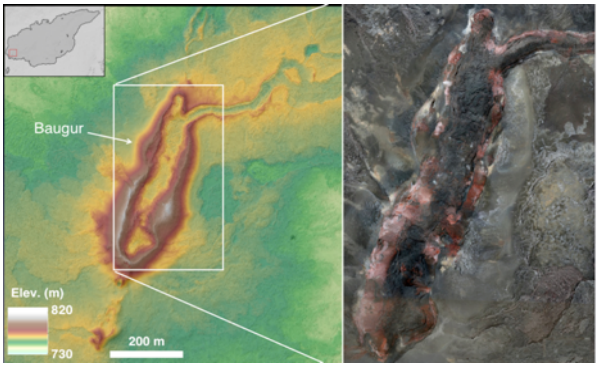

Figure 1. Terrain map (left) and orthophoto (right) of the 500-m-long spatter rampart that formed along the main vent. The channel feeding the majority of the flow units exits the vent to the NE. Inset is the outline of the Holuhraun lava field, with the vent area outlined by the red rectangle. North is up.

We acquired topographic data of the vent region post-eruption during the summers of 2015, 2016, 2018, and 2019 with a terrestrial laser scanner (TLS) and aerial photogrammetric surveys acquired using unmanned aerial systems (UAS) (**Fig. 1**) [7,8]. Centimeter-scale change detection maps were created from this time series using methods described in [9], allowing us to quantify the different types of mass wasting and the year-to-year average rates of erosion. We identified areas of episodic collapse on the interior slopes and diffusion effects on the exterior slopes, and discuss the earliest influences on erosion, such as slope instability, fumarolic activity, and degree of welding.

Spatter Rampart Construction: The morphology of vent edifices is primarily controlled by the intensity of fountaining. Other factors include the volatile content and composition of the magma, lava discharge rate, vent geometry, and duration of the eruption [2,3]. Unlike radially symmetric cinder cones, spatter ramparts form elongate pyroclastic deposits along a volcanic fissure [10]. Spatter is made of lava clasts that remain partially molten, or are hot enough upon deposition to still be deformable [11]. Spatter agglutinates as it is deposited [10], grading from loosely (tack) welded to tightly welded, where compaction and heat are high enough that individual clast boundaries are no longer distinct [11]. As the degree of welding increases (which is largely a function of accumulation rate), the boundaries between clasts become less distinct. A spatter rampart can thus form a more or less cohesive edifice with a morphology that is determined by the eruption history [12]. The amount of cohesion of the vent-proximal deposits has a direct effect on the rate of subsequent erosion.

Erosion of Vent Deposits: Models using morphometric parameters and diffusion equations have been developed for cinder cone construction and degradation [13–19]. These models do not directly apply to spatter ramparts due to differing material cohesion and subsequent stability [e.g., 12,20]. In most cases on Earth and other planetary surfaces where the eruption

was not witnessed, the initial form of the vent edifice is lost, leaving the degraded state to be used to infer eruption dynamics. Erosion models used to estimate ages also depend on assumptions about the initial morphology [15,17]. Without knowledge of the initial form and earliest morphological changes, this could lead to misinterpretation of eruption characteristics or relative age based on the current state of the vent edifice.

Results: High-resolution difference maps (2015–2016, 2016–2018, and 2018–2019) show two distinct types of erosion on the exterior and interior surfaces of Baugur .

Interior. Discrete sections of wall facing collapse in episodic rock fall events at higher elevations and on over-steepened slopes. The vertical extent of topographic change is on the order of meters, with most of the cumulative change from 2015–2019 being up to 6 m in the Z (vertical) direction (**Fig. 2,a–c)**. As the wall face retreats, the exposed surface remains oversteepened (**Fig. 2.d–f**). The rim has retreated horizontally and vertically by ~1.5 m in some places (**Fig. 2,g**). Over 2,400 m^3 of material has been removed from the upper 30 meters of the interior [8]. The material removed accumulates on ledges below the rim, building up talus slopes approaching the angle of repose for unconsolidated granular material (~35º). Wall material has not accumulated in quantity on the vent floor.

Exterior. The exterior slopes show exposures of spatter along the rim and upper portion of the rampart (slope ~45º), with interbedded spatter and scoria in the middle (slope ~34º), and scoria at the base (slope ~30º). Over the period of study (2015–2019), the exterior slopes changed little, with some measurable downslope accumulation of material of <20 cm. Diffusion processes may be occurring on the exterior slopes, but the changes are near the limits of the data.

Summary: We measured topographic changes over the first five years post-emplacement of a large spatter rampart in Iceland using high spatial resolution topography derived from TLS and UAS stereophotogrammetry. Analysis of the change detection time series shows two styles of erosion which are dependent on the initial deposition of the pyroclasts, cohesion, and slope stability. The earliest stages of degradation are dominated by discrete mass-wasting events on the interior walls. Diffusive processes occur on the exterior, but are hindered by the cohesive spatter deposits along the upper portion of the rim. Holuhraun is a useful analog to fissure vent edifices on other planets, where the age and degradation state are unknown [21]. The results of this study will provide improved understanding of how factors related to the construction of spatter deposits influence their degradation and morphologic evolution.

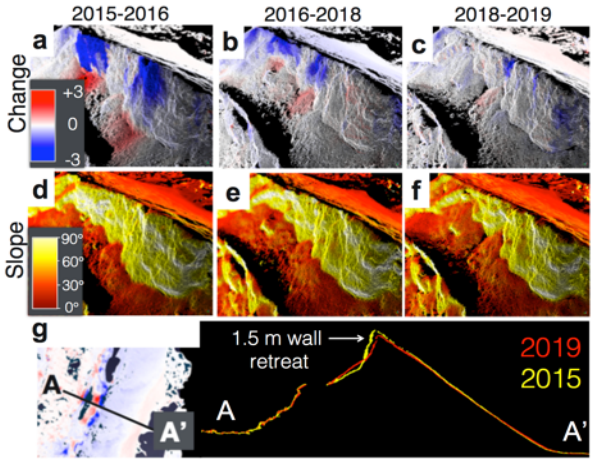

Figure 2. Detail of changes in the lidar data. View is of the interior eastern wall of Baugur. North is to the upper left. Scene is 40 m across. **a,b,c)** Difference maps in the Z-direction. Blue indicates negative topographic change (erosion). Red indicates deposition. Scale is in meters. **d,e,f)** Slope maps over a 3-meter baseline for 2015, 2016, and 2018 respectively. Black indicates gaps in the lidar data due to obscured view. **g)** Topographic profiles over the same location, from 2015 and 2019. Inset is aerial perspective of the profiles, north is up.

Acknowledgements: Field work was supported by NASA Goddard Instrument Field Team (GIFT) and by NASA PG&G Grant #NNX13AQ05G. S. Sutton was partially supported by NSF GRF Grant DGE-1746060.

References: [1] Wilson, L., Head, J.W. (1981) *JGR, 86:B4*, 2971–3001. [2] Head, J.W., Wilson, L. (1989) *JVGR, 37*, 261–271. [3] Riedel, C., et al. (*2003) JVGR, 127*, 121–152. [4] Höskuldsson, A., et al. (2016) *EGU Gen. Assy,* p. 13687. [5] Pedersen, G.B.M et al. (2017) *JVGR, 340*, 155–169. [6] Witt, T., et al. (2018) *Front. Earth Sci. 6*. [7] Hamilton, C. W. (2015), *Eos*, 96. [8] Richardson, J.A., et al. (2018) *AGU Fall Meeting*. [9] Lague, D., et al. (2013) *J. Photogram. and Rem. Sens., 82*, 10–26. [10] Valentine, G.A., Connor, C.B. (2015) *Ch. 23* in *The Encyclopedia of Volcanoes*, Academic Press, pp. 423–439. [11] Sumner, J., et al. (2005) *JVGR, 142*, 49–65. [12] Rader, E., et al. (2018) *Earth and Space Sci., 5*, 592–603. [13] Porter, S.C. (1972) *GSA Bull., 83*, 3607–3612. [14] Settle, M. (1979) *Amer. J. of Science, 279*, 1089–1107. [15] Pelletier, J.D., Cline, M.L. (2007) *Geology, 35:12*, 1067–1070. [16] Wood, C.A. (1980) *JVGR, 7*, 387–413. [17] Wood, C.A. (1980) *JVGR, 8*, 137–160. [18] Inbar, M. et al. (1994) *Geomorphology, 9*, 57–76. [19] Fornaciai, A. et al. (2010) *Bull. Volc., 72*, 1209–1222. [20] Rader, E., Geist, D. (2015) *JVGR, 304*, 287–293. [21] Richardson, J.A. et al. (2020) *LPS LI,* Abstract #1210.